Scientia Iranica B (2022) 29(6), 3107–3118

Sharif University of Technology
Scientia Iranica
Transactions B: Mechanical Engineering
http://scientiairanica.sharif.edu

Research Note

Influence of curvature-dependent channel walls on MHD peristaltic flow of viscous fluid with Hall currents and Joule dissipation

Saba[a], F.M. Abbasi[a], and S.A. Shehzad[b,*]

a. *Department of Mathematics, COMSATS University Islamabad, Islamabad 44000, Pakistan.*
b. *Department of Mathematics, COMSATS University Islamabad, Sahiwal 57000, Pakistan.*

Received 28 June 2021; received in revised form 21 April 2022; accepted 1 August 2022

KEYWORDS
Hall current;
Viscous fluid;
Peristaltic flow;
Joule dissipation;
Curvature dependent channel walls.

Abstract. The prime motive of this study is to assess the behavior of curvature-dependent channel boundaries on the Magnetohydrodynamic (MHD) peristaltic flow of viscous liquid with heat transportation effects via a curved channel. The analysis is reported by considering the Hall currents, Joule, and viscous dissipations effects. Further, no-slip momentum and thermal conditions are incorporated. Mathematical model is subjected to the implication of large wavelength and weaker magnetic Reynolds number schemes. Galilean transformation is used to convert the problem from laboratory frame into wave frame. The solution of the system of equations is executed by employing the numerical method ND solve (built-in command in Mathematica). The volume and mean flow rates are computed and examined. Graphical illustrations are provided to evaluate the nature of distinct constraints on velocity, temperature, and rate of heat transportation. Results show that the curvature constraint has significant impact on the mechanical and thermal features of the flow. The damping effects of the magnetic field improve the temperature and rate of heat transportation at the boundary. Moreover, a reduction in thermal transportation rate is noticed for the increased curvature constraint values.

1. Introduction

The continuous transport of body fluid through a distensible tube because of the change in pressure along the tube walls is known as peristaltic pumping. The peristaltic behavior of fluids has a potential role in distinct physiological processes. The physiological processes use the mechanism of peristalsis for the transport of fluid in biological systems. These processes involve the passage of food bolus via the esophagus, lymph motion in lymphatic vessels, discharge of waste material from the body, working of the digestive system, spermatic transport in the male reproductive system, the blood circulation in blood vessels, ovum motion in fallopian tubes, and digestive system functioning. Besides, the mechanism of peristalsis also exhibits importance in designing biomedical instruments like heart-lung dialysis machine, blood pumps, etc. The process of peristalsis is also used to prohibit the direct linkage of the liquid with pump components during the flow of corrosive fluids or purified fluids and as in finger/roller pumps. Further, this process is utilized in the transport of toxic fluids (in the nuclear industries, this mechanism is exploited in the transportation of toxic liquids). This phenomenon of

*. *Corresponding author.*
E-mail address: ali_qau70@yahoo.com (S.A. Shehzad)

doi: 10.24200/sci.2022.58621.5818

peristalsis has drawn the vital attention of researchers across the globe. Latham [1] first initiated the concept of peristalsis through an experimental study. Next, the mechanism of peristalsis has been investigated by several researchers with different approaches. The viscous fluid flow in a thick-walled viscoelastic pipe given specific flow and pressure conditions was analyzed by Whirlow and Rouleau [2]. Shapiro [3] studied the pumping of retrograde diffusion in the peristaltic waves. Shapiro et al. [4] introduced the lubrication theory model for peristaltic flow by considering the negligible effect of fluid inertia and wave number. Ali et al. [5] reported the thermal transportation aspects in viscid fluid flowing through a curved channel having wavy walls. Hayat and Abbasi [6] addressed the magnetized flow of third-order peristaltic fluid through a channel under slip and variable viscosity aspects. Numerical computations for the evaluation of micropolar peristaltic fluid motion in a curved channel were reported by Ali et al. [7]. Vajravelu et al. [8] elucidated the peristaltic transportation of Williamson liquid in an asymmetric channel by adopting the peristalsis wave train on the walls with distinct phases and amplitudes. The mathematical formulation for the peristaltic pumping of liquids mixtures through circular cylinders was executed by Mekheimer et al. [9]. Tripathi et al. [10] constructed a mathematical model to analyze the peristaltic flow of non-Newtonian physiological liquid via an asymmetric channel with a porous medium. Makinde and Reddy [11] disclosed the nature of magneto peristaltic movement of Casson fluid filling the porous space. Hayat et al. [12] addressed the entropy production phenomenon in Sisko nano liquid flow that fills non-Darcy porous space. The role of Brownian movement, Coriolis forces, and thermophoresis factor in the peristaltic movement of viscous liquid was studied by Mabood et al. [13].

Peristalsis with magnetohydrodynamic (MHD) plays a vital role in biomedical sciences. These effects are used in MRI (Magnetic Resonance Imaging) to detect and cure tumor and in magnetotherapy. MHD peristaltic transport is important because of its vital applications in biomedical science; few examples are MHD compressors utilize MRI to detect and cure tumors, ulceration, and urinary tract problems. Further, peristalsis through heat transportation is utilized in the process such as hemodialysis, oxygenation, hyperthermia, etc. The magnetic peristaltic transportation of Carreau fluid with the transfer of heat through convection was executed by Hayat et al. [14]. MHD peristaltic flow of Carreau-Yasuda (C-Y) fluid via a curved geometry under the consideration of slip condition was inspected by Abbasi et al. [15]. Rashidi et al. [16] examined the peristaltic movement of Casson blood fluid under heat mass transportation features. Asha and Sunitha [17] discussed impact of the Joule heating and magnetic force on Eyring-Powell blood fluid flow under suspension of nanoparticles passing through the non-uniform channel. The impact of endoscope on peristaltic transportation of couple stress liquid between co-axial tubes was addressed by Ramesh and Devakar [18]. Selimefendigil et al. [19] enlightened the magnetic field and convection aspects of nanofluid in a vertical cavity with a stretchy fin that is connected to its outer wall. Hayat et al. [20] elucidated the behavior of nanoparticles in irreversible flow of peristaltic fluid under second-order slip regime. Iqbal et al. [21] addressed the energy transportation of C-Y nanoliquid flow with radial magnetic force. Analysis of mass transportation in magnetized Casson fluid flowing over a starching/shrinking sheet was reported by Mahabaleshwar et al. [22]. Shah et al. [23] employed the shooting technique to analyze the magnetized entropy generation in stagnation-point flowing through an extendable Riga boundary with porous media. The impact of heat transfer on peristaltic Newtonian fluid across a porous conduit was investigated by Kiran et al. [24]. A theoretical analysis of thermal ignition in Oldroyd 8-constant liquid via a channel was introduced by Salawu et al. [25]. Shamshuddin et al. [26] reported the impact of transverse magnetic field and Hall current influences in non-Newtonian liquid flowing over an exponentially stretching sheet. Akbar et al. [27] addressed the impact of the Hall current on nanofluid flow having distinct nanoparticles through a straight channel with pulsating walls. Tripathi et al. [28,29] demonstrated the electroosmotic peristalsis of micro polar nanofluids with double diffusion and electro kinetically driven peristaltic movement of hybrid nanomaterials. Ranjit et al. [30] scrutinized the two-layered electroosmotic non-Newtonian fluid flowing in an asymmetric channel with velocity and thermal slip conditions. Selimefendigil and Chamkha [31] utilized the Finite Element Method (FEM) approach to mixed convected magneto hybrid nanofluid through a triangular cavity. Abdal et al. [32] reported the influence of thermal transportation in MHD bioconvective Maxwell nanofluid over a stretchable sheet with radiative heat flux, specific temperature, and thermal gradient conditions. Entropy production in magnetic stagnation point flow of tangent-hyperbolic nanomaterial with mass and thermal transportation was evaluated by Zhao et al. [33]. Hashmi et al. [34] investigated the simultaneous impact of magnetic dipole and mixed convection in reactive transportation of non-Newtonian material flowing over an extendable disk. Nazeer et al. [35] presented a comprehensive study on multi-phase Newtonian and non-Newtonian fluids over an inclined channel. Nisar et al. [36] reported the effect of Robin's condition and wall features on magnetized peristaltic motion of Eyring-Powell nanoliquid through radiative channel. Rao and Shamshuddin [37] investigated the time-dependent Hall current aspects in radiated chemically reacting liquid flow. Saba et al. [38] considered the simultaneous impacts of magnetic and electric fields on peristaltic flow of viscid fluid via curved channel. Peristaltically driven magnetized nanofluids under electric field via straight and curved geometries through different assumptions were studied by Akram et al. [39–41], because the curved geometries and curvature are ambiguously encountered in the physiological process and biological mechanism/studies. Curved surfaces are found in biological tissues. Curvature of tissues increased surface area required for nutrition absorption in the colon or gas exchange in the lungs. Many processes including cell mobility, stem cell formation, and disease progression can be influenced by curvature of the cells. Tissues in our body are unable to see and are aware of their environment and their shapes [42]. Many cellular processes, as well as tissue morphogenesis, pathology, and repair, are guided by physical cues in their environments according to recent studies. The nature of local geometries as an extracellular cue is one aspect that is gaining impetus. Understanding how geometries affect the tissue and cell function is critical to developing artificial scaffolds and ensuring a better understanding of tissue remodeling and growth. Surface curvature is the most basic description of local geometry, and a growing body of evidence shows that it has an impact on the spatiotemporal establishment of tissues and cells [43]. The impact of curvature and wall thickness on wall stress in a patient-specific electromechanical model of the left atrium was studied by Augustin [44]. The pulsating flow of viscous fluid flowing over a curved channel with thermal transport effects was discussed by Saba et al. [45].

Several investigations into peristalsis through different geometries subject to different physical effects exist in the literature. However, not enough scope of research has been found in the literature to investigate the peristaltic movement of fluid through a curved channel in which the curvature is engaged in the modeling of channel walls. Motivated from the above studies, the purpose here is to introduce a mathematical model that involves the effects of curvature-dependent channel boundaries on the peristaltic motion of viscous fluid via a curved channel. Further, the thermal transport, viscous dissipation, Joule dissipation, and Hall effects are also considered. It is noteworthy that effects of curvature-dependent channel walls have not received due attention in above-mentioned studies, thus providing an opportunity for further research in this direction, particularly for nano and hybrid nanofluids.

2. Statement of the problem

MHD peristalsis of viscous fluid via a curved channel with channel width "$2a$" bent in a circle centered at "O" and radius "R^*" is considered. The curvilinear coordinate system $(\tilde{R}, \tilde{X})$ is taken in such a manner that $\tilde{R}$-axis is chosen along radial direction, while $\tilde{X}$-axis is considered normal to it. The sinusoidal waves imposed on the channel boundaries account for fluid flow generation within a channel (see Figure 1). Both walls are kept at temperature "T_0". Mathematically, the channel walls of the present flow problem are defined as follows [45]:

$$\pm W\left(\tilde{X}, \tilde{t}\right) = \pm a \pm d \cos\left(\frac{2\pi}{\lambda}\left(\tilde{X} - s\tilde{t}\right)\right) + R^*. \quad (1)$$

Here, $\tilde{t}$, s, d, λ, and R^* represent the time, speed of the sinusoidal waves, amplitude, wavelength, and radius of the channel, respectively, whereas $+W$ and $-W$ characterize the above and lower boundaries of the channel, respectively.

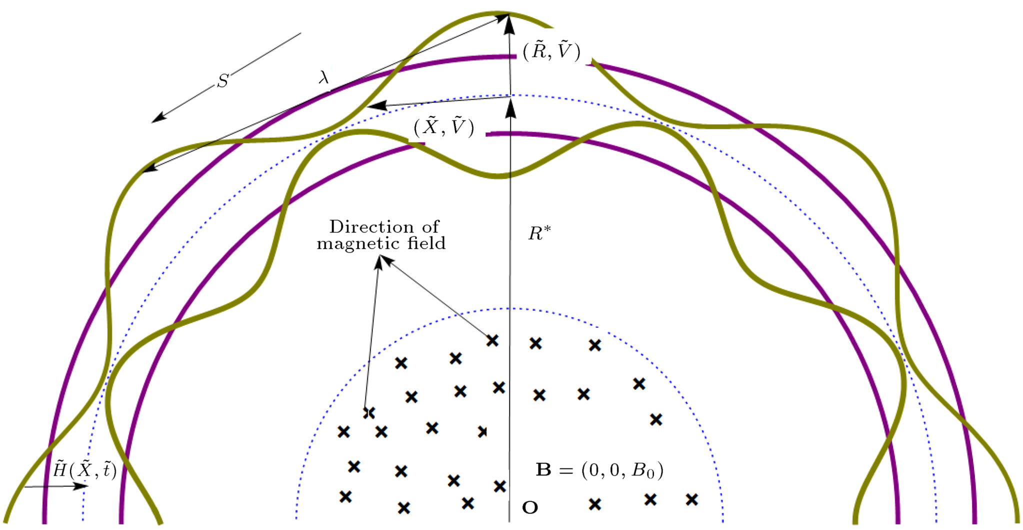

Figure 1. Geometry of the problem.

The applied magnetic field is defined as follows:

$$\mathbf{B} = (0, 0, B_0). \tag{2}$$

Mathematically, Ohm's law in the existence of Hall effects is given as follows [38]:

$$\mathbf{J} = \sigma\left(\mathbf{E} + \mathbf{V} \times \mathbf{B} - \frac{(\mathbf{J} \times \mathbf{B})}{en_e}\right). \tag{3}$$

Thus, the Lorentz force in the light of Eqs. (2) and (3) is defined as follows:

$$\mathbf{F} = \left(\frac{\sigma B_0^2}{1+m^2}\left(-\tilde{U}+m\tilde{V}\right), \frac{-\sigma B_0^2}{1+m^2}\left(\tilde{V}+m\tilde{U}\right), 0\right), \tag{4}$$

where σ, n_e, e, and m denote the electrical conductivity, free electron density, the charge on electron, and Hall parameter, respectively. The expressions that govern the fluid movement through the curved channel in a laboratory frame are defied as [5,45]:

$$\left(R^* + \tilde{R}\right)\frac{\partial \tilde{U}}{\partial \tilde{R}} + \tilde{U} + R^* \frac{\partial \tilde{V}}{\partial \tilde{X}} = 0, \tag{5}$$

$$\begin{aligned} &\rho\left(\frac{\partial \tilde{U}}{\partial \tilde{t}} + \tilde{U}\frac{\partial \tilde{U}}{\partial \tilde{R}} + \left(R^*\tilde{V}\frac{\partial \tilde{U}}{\partial \tilde{X}} - \tilde{V}^2\right)\frac{1}{\tilde{R}+R^*}\right) \\ &= -\frac{\partial \tilde{P}}{\partial \tilde{R}} + \frac{1}{\left(\tilde{R}+R^*\right)}\frac{\partial}{\partial \tilde{R}}\left(S_{\tilde{R}\tilde{R}}\left(\tilde{R}+R^*\right)\right) \\ &+ \frac{R^*}{\left(\tilde{R}+R^*\right)}\frac{\partial}{\partial \tilde{X}}S_{\tilde{R}\tilde{X}} - \frac{S_{\tilde{X}\tilde{X}}}{\left(\tilde{R}+R^*\right)} \\ &+ \sigma\frac{B_0^2}{1+m^2}\left[-\tilde{U} + m\tilde{V}\right], \end{aligned} \tag{6}$$

$$\begin{aligned} &\rho\left[\frac{\partial \tilde{V}}{\partial \tilde{t}} + \tilde{U}\frac{\partial \tilde{V}}{\partial \tilde{R}} + \left(R^*\frac{\partial \tilde{V}}{\partial \tilde{X}} + \tilde{U}\right)\frac{\tilde{V}}{R^*+\tilde{R}}\right] \\ &= -\frac{R^*}{R^*+\tilde{R}}\frac{\partial \tilde{P}}{\partial \tilde{X}} + \frac{1}{\left(R^*+\tilde{R}\right)^2}\frac{\partial}{\partial \tilde{R}}\left(\left(R^*+\tilde{R}\right)^2 S_{\tilde{R}\tilde{X}}\right) \\ &+ \frac{R^*}{\left(R^*+\tilde{R}\right)}\frac{\partial}{\partial \tilde{X}}S_{\tilde{X}\tilde{X}} - \frac{\sigma B_0^2}{1+m^2}\left(\tilde{V}+m\tilde{U}\right), \end{aligned} \tag{7}$$

$$\rho C_p\left[\frac{\partial}{\partial \tilde{t}} + V \cdot \nabla\right] T = K\nabla^2 T + S \cdot L + \frac{1}{\sigma} J \cdot J. \tag{8}$$

Here, $\tilde{P}(\tilde{R}, \tilde{X}, \tilde{t})$, ρ, C_p, B_0, m, and K denote the fluid's pressure, density, specific heat at constant pressure, strength of applied magnetic field, Hall parameter, and thermal conductivity, respectively. Further, we have:

$$S_{\tilde{R}\tilde{R}} = 2\mu\frac{\partial}{\partial \tilde{R}}\tilde{U},$$

$$S_{\tilde{X}\tilde{R}} = \mu\left(\frac{\partial \tilde{V}}{\partial \tilde{R}} + \frac{1}{\left(\tilde{R}+R^*\right)}\left(R^*\frac{\partial \tilde{U}}{\partial \tilde{X}} - \tilde{V}\right)\right),$$

$$S_{\tilde{X}\tilde{X}} = \mu\left(\frac{1}{\tilde{R}+R^*}\left(2R^*\frac{\partial \tilde{V}}{\partial \tilde{X}} + 2\tilde{U}\right)\right),$$

$$\nabla = \frac{\partial}{\partial \tilde{R}} + \frac{1}{R^*+\tilde{R}}\frac{\partial}{\partial \tilde{X}},$$

$$\nabla^2 = \frac{\partial^2}{\partial \tilde{R}^2} + \frac{1}{R^*+\tilde{R}}\frac{\partial}{\partial \tilde{R}} + \frac{1}{\left(R^*+\tilde{R}\right)^2}\frac{\partial^2}{\partial \tilde{X}^2},$$

$$\begin{aligned} tr(S \cdot L) = \mu\Bigg(&2\left(\frac{\partial \tilde{U}}{\partial \tilde{R}}\right)^2 \\ &+ \left(\frac{\partial \tilde{V}}{\partial \tilde{R}} + \frac{1}{R^*+\tilde{R}}\left(R^*\frac{\partial \tilde{U}}{\partial \tilde{X}} - \tilde{V}\right)\right)^2 \\ &+ \frac{2}{\left(R^*+\tilde{R}\right)^2}\left(R^*\frac{\partial \tilde{V}}{\partial \tilde{X}} + \tilde{U}\right)^2\Bigg), \end{aligned}$$

$$\frac{1}{\sigma}J \cdot J = \frac{\sigma B_0^2}{1+m^2}\tilde{V}^2. \tag{9}$$

The following transformation was considered to convert the above expressions from laboratory into the wave frame [10]:

$$\tilde{R} = \tilde{r}, \qquad \tilde{X} = \tilde{x} + s\tilde{t}, \qquad \tilde{P}\left(\tilde{R}, \tilde{X}, \tilde{t}\right) = \tilde{p}\left(\tilde{r}, \tilde{x}\right),$$

$$\tilde{V}\left(\tilde{R}, \tilde{X}, \tilde{t}\right) = \tilde{v}(\tilde{r}, \tilde{x}) + s, \qquad \tilde{U}\left(\tilde{R}, \tilde{X}, \tilde{t}\right) = \tilde{u}\left(\tilde{r}, \tilde{x}\right). \tag{10}$$

Eqs. (5)–(8) take the following form after employing Eqs. (9) and (10):

$$\left(\tilde{r} + R^*\right)\frac{\partial \tilde{u}}{\partial \tilde{r}} + \tilde{u} + R^*\frac{\partial}{\partial \tilde{x}}\left(\tilde{v} + s\right) = 0, \tag{11}$$

$$\begin{aligned} &\rho\left[\tilde{u}\frac{\partial \tilde{u}}{\partial \tilde{r}} + \left(R^*\frac{\partial \tilde{u}}{\partial \tilde{x}} - (\tilde{v}+s)\right)\frac{(\tilde{v}+s)}{\tilde{r}+R^*}\right] \\ &= -\frac{\partial \tilde{p}}{\partial \tilde{r}} + \frac{\mu}{(\tilde{r}+R^*)}\frac{\partial}{\partial \tilde{r}}\left(2\left(\tilde{r}+R^*\right)\left(\frac{\partial \tilde{u}}{\partial \tilde{r}}\right)\right) \\ &+ \frac{R^*\mu}{(\tilde{r}+R^*)}\frac{\partial}{\partial \tilde{r}}\left(\frac{\partial(\tilde{v}+s)}{\partial \tilde{r}}\right. \\ &\left.+ \frac{1}{(\tilde{r}+R^*)}\left(R^*\frac{\partial \tilde{u}}{\partial \tilde{x}} - (\tilde{v}+s)\right)\right) \end{aligned}$$

$$- \frac{\mu}{(\tilde{r}+R^*)^2}\left(2R^*\frac{\partial(\tilde{v}+s)}{\partial\tilde{x}}+2\tilde{u}\right)$$

$$+\sigma\frac{B_0^2}{1+m^2}\left[-\tilde{u}+m(\tilde{v}+s)\right], \tag{12}$$

$$\rho\left[\tilde{u}\frac{\partial\tilde{v}}{\partial\tilde{r}}+\frac{1}{\tilde{r}+R^*}\left(R^*(\tilde{v}+s)\frac{\partial\tilde{v}}{\partial\tilde{x}}+(\tilde{v}+s)\tilde{u}\right)\right]$$

$$=-\frac{R^*}{R^*+\tilde{r}}\frac{\partial\tilde{p}}{\partial\tilde{x}}+\frac{\mu}{(R^*+\tilde{r})^2}\frac{\partial}{\partial\tilde{r}}\Bigg((R^*+\tilde{r})^2$$

$$\left(\frac{\partial(\tilde{v}+s)}{\partial\tilde{r}}+\frac{R^*}{(\tilde{r}+R^*)}\frac{\partial\tilde{u}}{\partial\tilde{x}}-\frac{\tilde{v}+s}{\tilde{r}+R^*}\right)\Bigg)$$

$$+\frac{R^*\mu}{(R^*+\tilde{r})}\frac{\partial}{\partial\tilde{x}}\left(\frac{2R^*}{\tilde{r}+R^*}\frac{\partial(\tilde{v}+s)}{\partial\tilde{x}}+2\frac{\tilde{u}}{\tilde{r}+R^*}\right)$$

$$-\frac{\sigma B_0^2}{1+m^2}\left((\tilde{v}+s)+m\tilde{u}\right), \tag{13}$$

$$\rho C_p\left[\tilde{u}\frac{\partial T}{\partial\tilde{r}}+\frac{R^*}{R^*+\tilde{r}}(\tilde{v}+s)\frac{\partial T}{\partial\tilde{x}}\right]$$

$$=K\left[\frac{\partial^2 T}{\partial\tilde{r}^2}+\frac{1}{R^*+\tilde{r}}\frac{\partial T}{\partial\tilde{r}}+\left(\frac{R^*}{R^*+\tilde{r}}\right)^2\frac{\partial^2 T}{\partial\tilde{x}^2}\right]$$

$$\mu\Bigg(2\left(\frac{\partial\tilde{u}}{\partial\tilde{r}}\right)^2+\Bigg(\frac{\partial}{\partial\tilde{r}}(\tilde{v}+s)+\frac{R^*}{R^*+\tilde{r}}\left(\frac{\partial\tilde{u}}{\partial\tilde{x}}\right)$$

$$-\frac{(\tilde{v}+s)}{R^*+\tilde{r}}\Bigg)^2+2\left(\frac{R^*}{R^*+\tilde{r}}\left(\frac{\partial(\tilde{v}+s)}{\partial\tilde{x}}\right)+\frac{\tilde{u}}{R^*+\tilde{r}}\right)^2\Bigg)$$

$$+\frac{\sigma B_0^2}{1+m^2}(\tilde{v}+s)^2. \tag{14}$$

Dimensionless variables [44]:

$$w=\frac{\pm W}{a},\qquad Re=\frac{\rho s a}{\mu_0},\qquad y=\frac{\tilde{r}}{a},$$

$$\delta=\frac{a}{\lambda},\qquad p=\frac{a^2\tilde{p}}{s\lambda\mu_0},\qquad m=\frac{\sigma B_0}{en_e},$$

$$k=\frac{R^*}{a},\qquad \theta=\frac{T-T_0}{T_0},\qquad x=\frac{\tilde{x}}{\lambda},$$

$$u=\frac{\tilde{u}}{s},\qquad Br=\frac{\mu_0 s^2}{kT_0},\qquad v=\frac{\tilde{v}}{s},$$

$$b=\frac{d}{a},\qquad M^2=\frac{\sigma B_0^2 a}{\mu_0},\qquad u=\frac{\partial\psi}{\partial x}\frac{k\delta}{k+y},$$

$$v=-\frac{\partial\psi}{\partial y}. \tag{15}$$

After using the above-mentioned nondimensional variables, negligible Reynolds number, and wave number assumptions, Eq. (11) is satisfied identically and Eqs. (12)–(14) become:

$$\frac{\partial p}{\partial x}=-\frac{1}{k(k+y)}\frac{\partial}{\partial y}\Bigg((k+y)^2\Bigg(\frac{1}{k+y}\left(1-\frac{\partial\psi}{\partial y}\right)$$

$$+\frac{\partial^2\psi}{\partial y^2}\Bigg)\Bigg)-(k+y)\frac{M^2}{k(1+m^2)}\left(1-\frac{\partial\psi}{\partial y}\right), \tag{16}$$

$$\frac{\partial p}{\partial y}=0, \tag{17}$$

$$\frac{\partial^2\theta}{\partial y^2}+\frac{1}{y+k}\frac{\partial\theta}{\partial y}+\mathrm{Br}\left(\frac{\partial^2\psi}{\partial y^2}+\frac{1}{k+y}\left(1-\frac{\partial\psi}{\partial y}\right)\right)^2$$

$$+\mathrm{Br}\left(\frac{M^2}{1+m^2}\right)\left(1-\frac{\partial\psi}{\partial y}\right)^2=0. \tag{18}$$

Cross differentiation of Eqs. (16) and (17) provides the following equation:

$$\frac{\partial}{\partial y}\left(-\frac{1}{k(k+y)}\frac{\partial}{\partial y}\left(\left(\frac{1}{y+k}\left(1-\frac{\partial\psi}{\partial y}\right)+\frac{\partial^2\psi}{\partial y^2}\right)(y+k)^2\right)\right)$$

$$-\frac{\partial}{\partial y}\left(\frac{M^2(k+y)}{k(1+m^2)}\left(1-\frac{\partial\psi}{\partial y}\right)\right)=0. \tag{19}$$

Here, the non-dimensional quantities θ, m, M, k, b, ψ, p, Br, and Re characterize the temperature, Hall parameter, Hartman number, curvature parameter, wave amplitude, stream function, pressure, Brinkman, and Reynolds number, respectively.

In the fixed and wave frames, the volume flow rates are given as:

$$Q^*=\int_{-W}^{+W}\tilde{V}\left(\tilde{R},\tilde{X},\tilde{t}\right)d\tilde{R},\qquad q^*=\int_{-w}^{+w}\tilde{v}(\tilde{r},\tilde{x})\,d\tilde{r}. \tag{20}$$

The flow rates in wave and laboratory frames are linked as follows:

$$Q^*=q^*+2sw(x).$$

Hence, the mean flow rate can be written as [44]:

$$Q^{**}=q^*+2as+2sR^*. \tag{21}$$

Dimensionless pattern of flow rates in wave and laboratory frames is given below:

$$\eta=F+2+2k. \tag{22}$$

The dimensionless pattern of peristaltic walls and boundary conditions is described as:

$$\pm w(x)=\pm 1\pm b\cos(2\pi x)+k. \tag{23}$$

$$\psi[-w] = \frac{F}{2}, \qquad \psi[w] = -\frac{F}{2},$$

$$\frac{\partial \psi}{\partial y}[\pm w] = 1, \qquad \theta[\pm w] = 0. \tag{24}$$

3. Solution methodology

Eqs. (18) and (19) with boundary conditions (24) were solved numerically with the aid of the Built-in numerical solver NDSolve in Mathematica 11. The step size for these computations is chosen as 0.01 for variations in x and y. To test numerical results, the comparison of a sub-case of the present study with analytical results obtained from an existing study [5] is presented in Tables 1 and 2, and both are found in good agreement.

4. Results and discussion

This section is prepared to evaluate the numerical outcomes through graphs. The effects of involved sundry parameters on fluid's velocity, temperature, and thermal transport rate at the channel wall are plotted and physically interpreted.

4.1. Velocity profile

Figures 2–5 depict the changes in axial velocity "$V(y)$" for the different involved sundry parameters such as the dimensionless flow rate "η", Hartmann number "M", Hall constraint "m", and curvature parameter "k". These figures indicate that the velocity has parabolic curves with the highest velocity existing near the middle of the channel and these curves satisfy the boundary conditions. Figure 2 expresses that $\eta = 7.5$ is the critical flow rate and it is also the minimum flow rate to continue the fluid flow within a curved channel

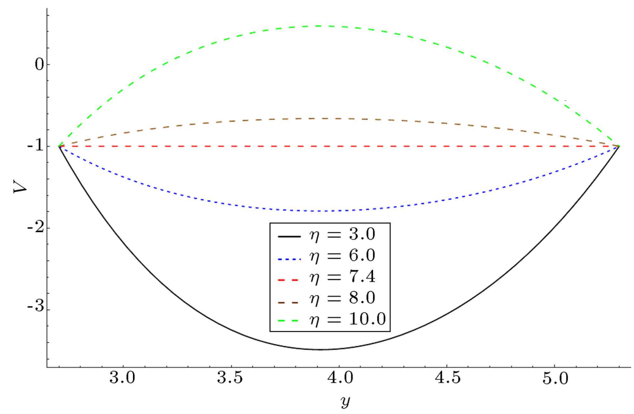

Figure 2. Velocity curves for η when $m = 2$, $d = 0.3$, $M = 2$, $Br = 2$, $k = 4$, and $x = 0$.

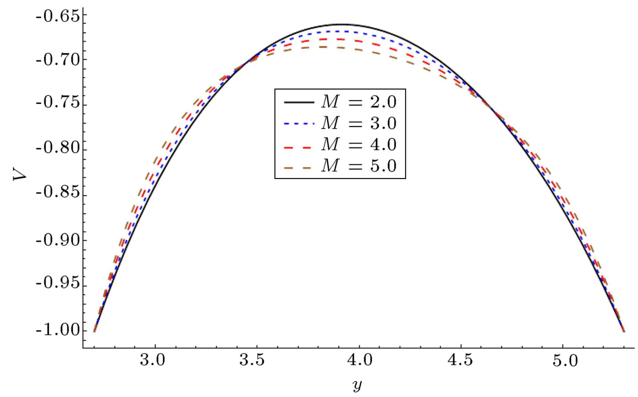

Figure 3. Velocity curves for M when $m = 2$, $\eta = 8$, $d = 0.3$, $Br = 2$, $k = 4$, and $x = 0$.

having curvature-dependent channel boundaries. It is observed that the velocity graphs are concave up and concave down with the highest and lowest values of velocity arising close to the middle of the curved channel for $\eta > 7.5$ and $\eta < 7.5$, respectively. Further,

Table 1. Comparison between exact [10] and numerical results when $x = 0$, $k = 3$, $d = 0.6$, $\eta = 2$, $Br = 2$, and $y = 0$ (center of channel).

Temperature "θ"	Exact solution	Numerical solution	Error
Curvature $k = 3$	2.1417356921458826	2.141735716954361	$2.48084783 \times 10^{-8}$
4	1.8489843676728128	1.848984325697747	$4.19750658 \times 10^{-8}$
5	1.7201816733646638	1.7201815944967997	$7.88678640 \times 10^{-8}$
$Br = 2$	2.141735692146792	2.141735716954361	$2.48075688 \times 10^{-8}$
3	3.2126035382201863	3.2126036240324156	$8.58122293 \times 10^{-8}$
4	4.283471384293584	4.28347151805571	1.3376212×10^{-7}

Table 2. Comparison between exact and numeric solutions at different values of curvature parameter.

Curvature parameter	Exact solution	Numerical solution	Error
$k = 2$	−0.4503693110499591	−0.4503693138950907	2.84513×10^{-9}
3	−0.4719977215329828	−0.4719977218822102	3.49227×10^{-10}
4	−0.4820714866459177	−0.4820714863988828	2.47034×10^{-10}

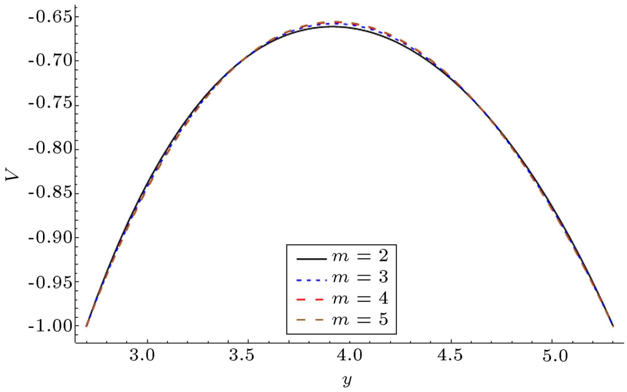

Figure 4. Velocity curves for m when $\eta = 8$, $d = 0.3$, $M = 2$, $Br = 2$, $k = 4$, and $x = 0$.

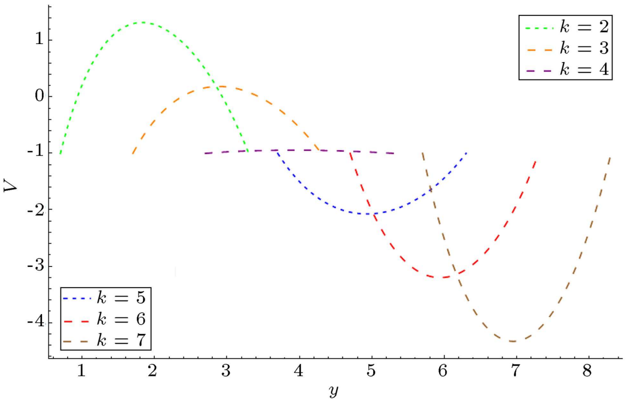

Figure 5. Velocity curves for k when $\eta = 7.5$, $d = 0.3$, $m = 2$, $Br = 2$, $M = 2$, and $x = 0$.

an increase and a decline in the velocity are noted with an increment in "η" above and below the critical value, respectively. Figure 3 presents the reduction of fluid velocity closest to the channel center for rising "M". However, a reverse impact is observed near channel walls. It is because the Lorentz force (i.e., resistive force) is enhanced by increasing the strength of the applied magnetic field. The axial velocity variation for distinct "m" values is shown in Figure 4. It is discovered that axial velocity is directly proportional to "m", as it is evident from the Hall effect formula that the Joule heating effect decreases at larger values of "m"; thus, the damping effects of Lorentz force are also reduced. The axial velocity retards at higher values of "k". The central axis moved forward at higher values of "k". This is because of the existence of "k" in the mathematical modeling of channel walls. Further, the velocity curves show a concave up behavior for $\eta > 7.5$ and $k > 4$. This indicates that the value of η should be greater than its critical value to maintain channel flow at large values of curvature parameter (see Figure 5).

4.2. Temperature profile and thermal transport rate

The temperature profile "θ" with respect to "y" at

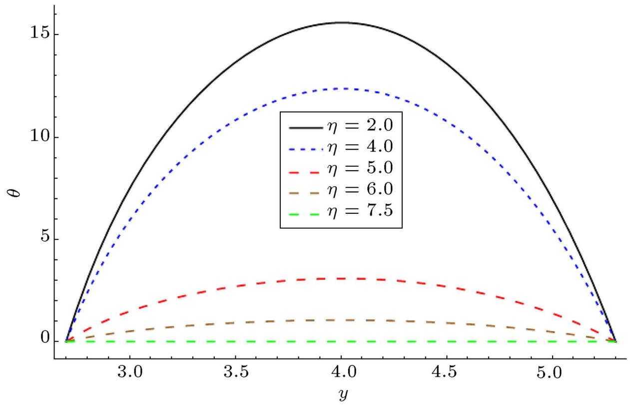

Figure 6a. Temperature curves for η when $m = 2$, $d = 0.3$, $M = 2$, $Br = 2$, $k = 4$, and $x = 0$.

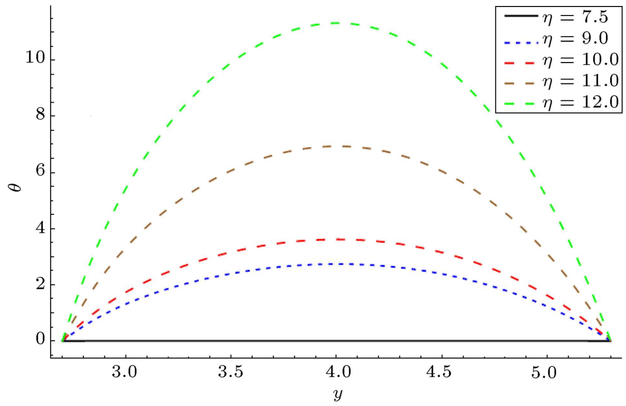

Figure 6b. Temperature curves for η when $m = 2$, $d = 0.3$, $Br = 2$, $M = 2$, $k = 4$, and $x = 0$.

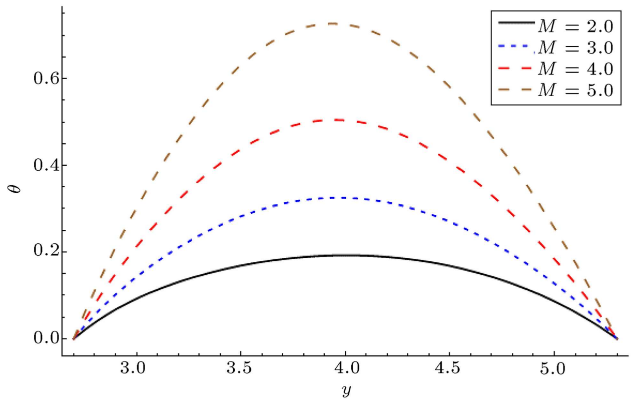

Figure 7. Temperature curves for M when $m = 2$, $d = 0.3$, $\eta = 8$, $Br = 2$, $k = 4$, and $x = 0$.

distinct values of sundry parameters is plotted in Figures 6–10. It is noted that "θ" graphs are also a parabolic form with the highest temperature occurring close to the middle of the curved geometry. Figures 6a and 6b reveal that at "$\eta > 7.5$", the rise of temperature profile is accountable with a rise in "η". However, at "$\eta < 7.5$", the decreasing behavior of temperature is visualized for enlarging "η". Figure 7 reports an augmentation in temperature with an enhancement in

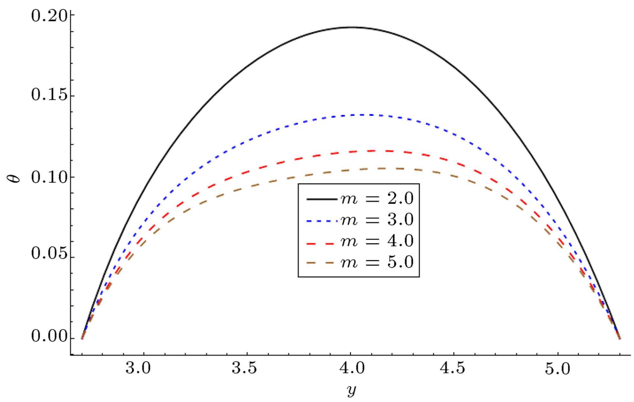

Figure 8. Temperature curves for m when $\eta = 8$, $d = 0.3$, $M = 2$, $Br = 2$, $k = 4$, and $x = 0$.

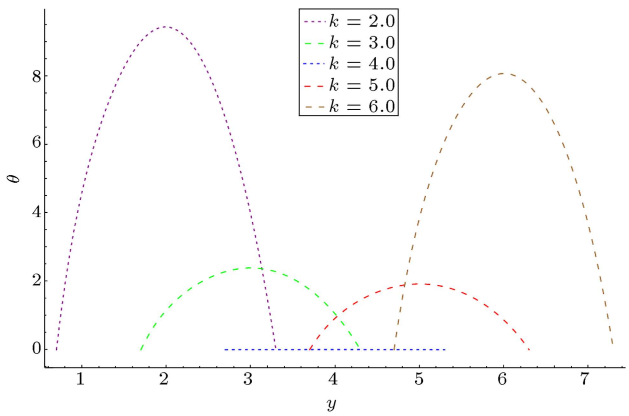

Figure 9. Temperature curves for k when $m = 2$, $d = 0.3$, $M = 2$, $Br = 2$, $\eta = 7.5$, and $x = 0$.

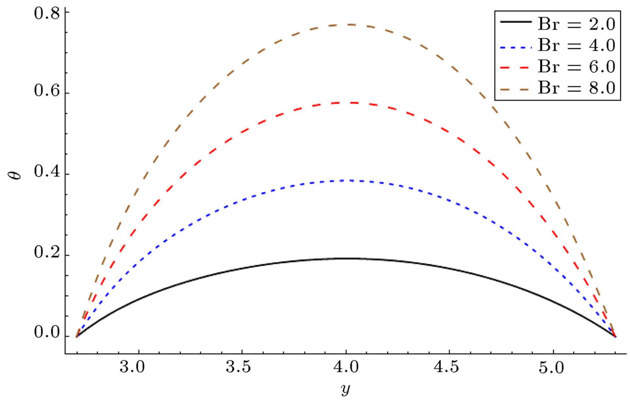

Figure 10. Temperature curves for Br when $m = 2$, $d = 0.3$, $M = 2$, $k = 4$, $\eta = 8$, and $x = 0$.

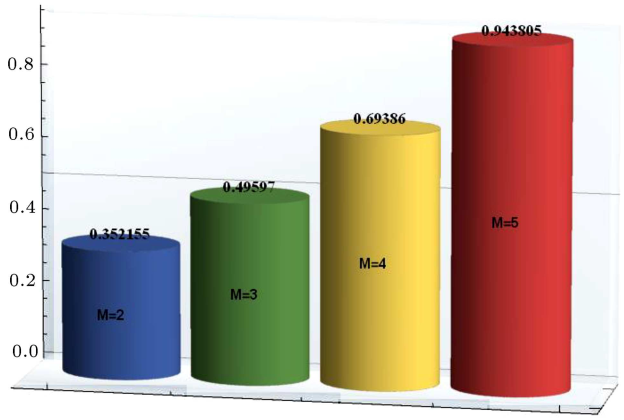

Figure 11. Thermal transport rate at the boundary for M when $m = 2$, $d = 0.3$, $\eta = 8$, $Br = 2$, $k = 4$, and $x = 0$.

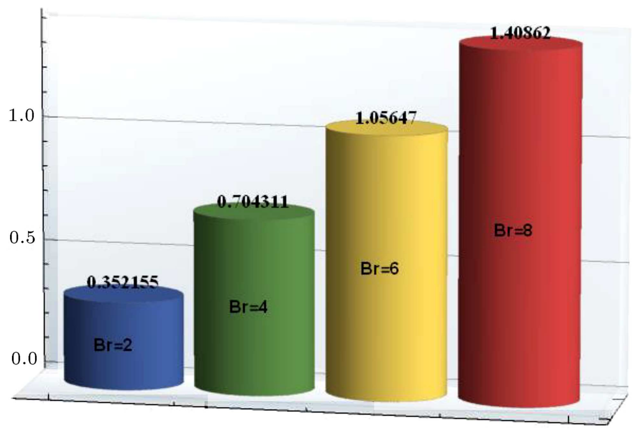

Figure 12. Thermal transport rate at the boundary for Br when $m = 2$, $d = 0.3$, $M = 2$, $\eta = 8$, $k = 4$, and $x = 0$.

"M". This increase in temperature profile is because of the resisting nature of magnetic force (physically, due to the Joule heating effects (i.e., heat dissipation improved)). Figure 8 defines a reduction in the fluid's temperature with a rise in "m". This is because an increase in "m" lowers the fluid's thermal conductivity and, thus, reduces the resistive effects of Lorentz force. Moreover, it is found that at smaller values of "m", the temperature profile tends to maintain symmetry near the central axis. Figure 9 shows that "$k = 4$" is the critical number of the curvature constraint. In the case of "$k > 4$", temperature of fluid increases with the enhancement of curvature constraint. A reverse trend is observed in the temperature profile of fluid below the critical value of "k" with an increment in "k". A rise in the values of "Br" causes an enhancement in the viscous dissipation effects and, thus, increases the fluid temperature, as depicted in Figure 10.

The nature of the involved flow constraints on $-\theta'(w)$ was executed, as can be seen in Figures 11–15. Figures 11 and 12 show that "$-\theta'[w]$" is proportional to "M" and "Br". Figure 13 indicates a decrement in the thermal transport rate at growing values of "m". Figure 14 shows that below the critical value of flow rate, the heat transfer rate rises with a reduction in "η"; however, above the critical value of the flow rate, the heat transmission rate increased with an increment in "η". Figures 15a and 15b reveal that when "$k > 4$", heat transfer rate is proportional to "k", while a decrease in the thermal transfer rate is found with a rise in "k", respectively.

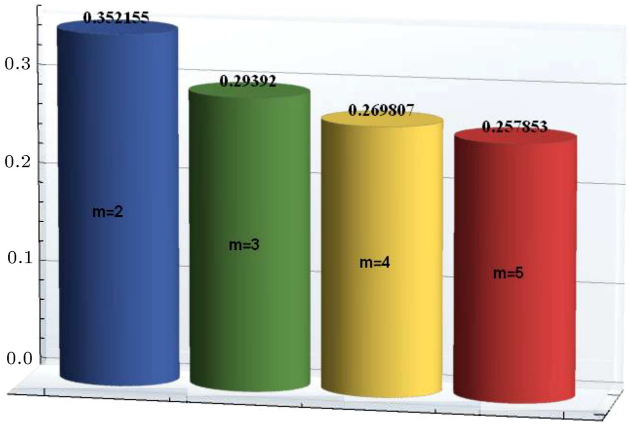

Figure 13. Thermal transport rate at the boundary for m when $M = 2$, $d = 0.3$, $\eta = 8$, $Br = 2$, $k = 4$, and $x = 0$.

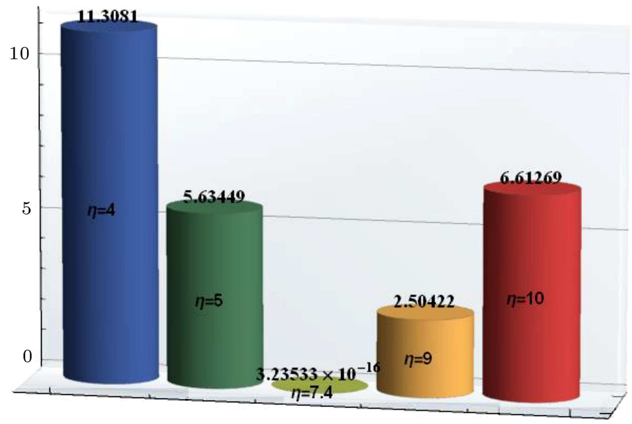

Figure 14. Thermal transport rate at the boundary for η when $m = 2$, $d = 0.3$, $M = 2$, $Br = 2$, $k = 4$, and $x = 0$.

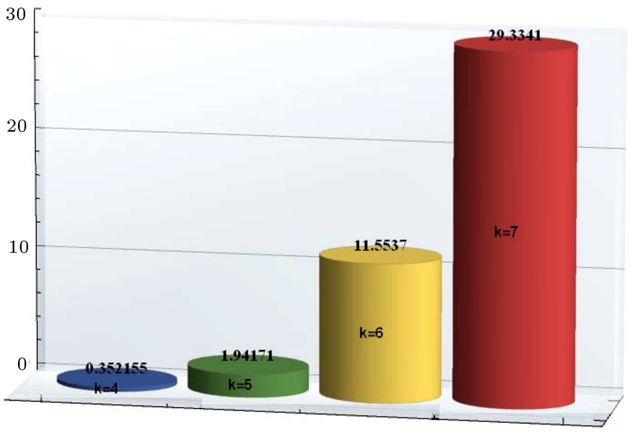

Figure 15a. Thermal transport rate at the boundary for k when $m = 2$, $d = 0.3$, $\eta = 8$, $Br = 2$, $M = 2$, and $x = 0$.

The comparison of the numerical results of a limiting case of the present study with exact solutions obtained by Ali et al. [5] for temperature and velocity profiles at different values of the involved parameters at the center of the channel is given through Tables 1 and 2. It is noted that the findings of this investigation are consistent with those of earlier research.

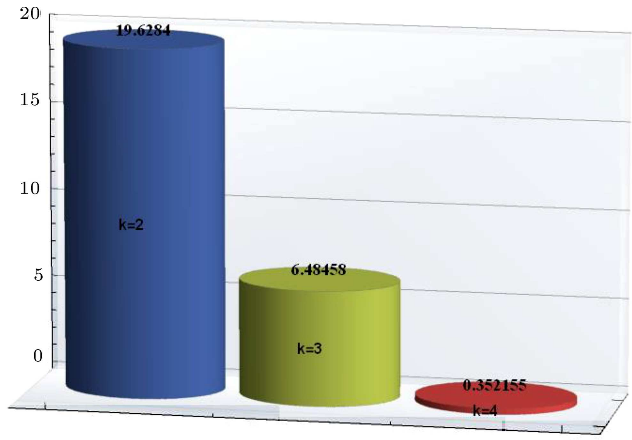

Figure 15b. Thermal transport rate at the boundary for k when $m = 2$, $d = 0.3$, $\eta = 8$, $Br = 2$, $M = 4$, and $x = 0$.

5. Conclusions

The effect of curvature-dependent channel boundaries on the peristaltic movement of viscous liquid through curved channel with Hall, Joule, and viscous dissipation effects was investigated in this study. The following key points are derived from the above discussion:

- Above and below the critical value flow rate, an increment in the axial velocity was achieved against the augmented flow rate;
- A rise in Hartmann number caused a drop in velocity profile. However, increase in axial velocity was found at the greater Hall constraint values;
- The velocity profile demonstrated that "$k = 4$" was the critical number of curvature constraint. It is noted that below and above the critical number of curvature constraint, the fluid velocity reduces with an increment in the curvature parameter;
- Below the critical value of the flow rate, a decrease in "η" resulted in the augmentation of temperature profile. However, above the critical value of flow rate, fluid temperature increased with a rise in "η";
- Below the critical value of curvature parameter, a reduction in temperature profile was found with increase in the value of "k". However, a reverse behavior is noted above the critical value of curvature parameter;
- Thermal transport rate increased with a rise in "M" and "Br";
- Thermal transmission rate declined against higher "m" values.

Nomenclature

$2a$	Channel width
F	Dimensionless flow rate in wave frame

m	Hall parameter
q^*	Volume flow rate in moving frame
(u, v)	Velocity components in wave frame
b	Dimensionless wave amplitude
J	Current density (Am^{-2})
n_e	Free electron density
R^*	Radius
Br	Brinkman number
B_0	Strength of magnetic field (Am^{-1})
K	Thermal conductivity (W/mk)
$\tilde{P}(\tilde{R}, \tilde{X}, \tilde{t})$	Pressure in stationary frame
s	Wave speed (ms^{-1})
$\tilde{W}(\tilde{X}, \tilde{t})$	Peristaltic wall
c_p	Specific heat ($\mathrm{Jkg}^{-1}\mathrm{k}^{-1}$)
k	Curvature parameter
$p(r, x)$	Pressure in wave frame
$\tilde{t}$	Time
$w(x)$	Dimensionless peristaltic wall
e	Charge on electron
M	Hartmann number
Q^*	Volume flow rate in fixed frame ($\mathrm{m}^3\mathrm{s}^{-1}$)
$\left(\tilde{U}, \tilde{V}\right)$	Velocity components in fixed frame
$\left(\tilde{R}, \tilde{X}\right)$	Curvilinear coordinate

Greek letters

λ	Wavelength
ψ	Stream function
σ	Electrical conductivity
ρ	Fluid density
θ	Dimensionless temperature
η	Dimensionless flow rate in fixed frame
μ	Dynamic viscosity

References

1. Latham, T.W., *Fluid Motion in Peristaltic Pump*, MIT, Cambridge MA (1966).
2. Whirlow, D.K. and Rouleau, W.T. "Peristaltic flow of viscous liquid in thick-walled elastic tube", *Math. Biosci.*, **27**, pp. 355–370 (1967).
3. Shapiro, A.H. "Pumping and retrograde diffusion in peristaltic waves", *Proc. Workshop Ureteral Ref.*, pp. 109–126 (1967).
4. Shapiro, A.H., Jaffrin, M.Y., and Weinberg, S.L. "Peristaltic pumping with long wavelength at low Reynolds number", *J. Fluid Mech.*, **37**, pp. 799–825 (1969).
5. Ali, N., Sajid, M., Javed, T., et al. "Heat transfer analysis of peristaltic flow in a curved channel", *Int. J. Heat Mass Transf.*, **53**, pp. 3319–3325 (2010).
6. Hayat, T. and Abbasi, F.M. "Variable viscosity effects on peristaltic motion of a third order fluid", *Int. J. Numer. Methods Fluids*, **67**, pp. 1500–1515 (2011).
7. Ali, N., Sajid, M., Javed, T., et al. "An analysis of peristaltic flow of micropolar fluid in a curved channel", *Chin. Phys. Lett.*, **28**, Article ID 014704 (2011).
8. Vajravelu, K., Sreenadh, S., Rajanikanth, K., et al. "Peristaltic transport of a Williamson fluid in asymmetric channel with permeable walls", *Non-Liner Anal. Real world Appl.*, **13**, pp. 2804–2822 (2012).
9. Mekheimer, K.S., Abd Elmaboud, Y., and Abdellateef, A. "Particulate suspension flow induced by sinusoidal peristaltic waves through eccentric cylinders: thread annular", *Int. J. Biomath.*, **6**, Article ID 1350026 (2013).
10. Tripathi, D., Bég, O.A., Gupta, P.K., et al. "DTM simulation of peristaltic viscoelastic biofluid flow in asymmetric porous media: a digestive transport model", *J. Bionic Eng.*, **12**, pp. 643–655 (2015).
11. Makinde, O.D. and Reddy, M.G. "MHD peristaltic slip flow of Casson fluid and heat transfer in channel filled with a porous medium", *Sci. Iran.*, **26**, pp. 2342–2355 (2019).
12. Hayat, T., Ahmed, B., Abbasi, F.M., et al. "Peristaltic radiative flow of Sisko nanomaterial with entropy generation and modified Darcy's law", *J. Therm. Anal. Calorim.*, **147**, pp. 409–419 (2020).
13. Mabood, F., Abbasi, A., Farooq, W., et al. "Thermophoresis effect on peristaltic flow of viscous nanofluid in rotating frame", *J. Therm. Anal. Calorim.*, **143**, pp. 2621–2635 (2021).
14. Hayat, T., Zahir, H., Alsaedi, A., et al. "Hall current and Joule heating effects on peristaltic flow of viscous fluid in a rotating channel with convective boundary conditions", *Resul. Phys.*, **7**, pp. 2831–2836 (2017).
15. Abbasi, F.M., Saba, and Shehzad, S.A. "Heat transfer analysis for peristaltic flow of Carreau-Yasuda fluid through a curved channel with radial magnetic field", *Int. J. Heat Mass Transf.*, **115**, pp. 777–783 (2017).
16. Rashidi, M.M., Yang, Z., Bhatti, M.M., et al. "Heat, and mass transfer analysis on MHD blood flow of Casson fluid model due to peristaltic wave", *Therm. Sci.*, **22**, pp. 2439–2448 (2018).
17. Asha, S.K. and Sunitha, G. "Effect of joule heating and MHD on peristaltic blood flow of Eyring-Powell nanofluid in a non-uniform channel", *J. Taibah Uni. Sci.*, **13**, pp. 155–168 (2019).
18. Ramesh, K. and Devakar, M. "Effect of endoscope on the peristaltic transport of a couple stress fluid with heat transfer: Application to biomedicine", *Nonlinear Eng.*, **8**, pp. 619–629 (2019).

19. Selimefendigil, F., Oztop, H.F., and Chamkha, A.J. "MHD mixed convection in a nanofluid filled vertical lid-driven cavity having a flexible fin attached to its upper wall", *J. Therm. Anal. Calorim.*, **135**, pp. 325–340 (2019).
20. Hayat, T., Nawaz, S., and Alsaedi, A. "Entropy generation analysis of peristaltic flow of magneto-nanoparticles suspended in water under second-order slip conditions", *Sci. Iran.*, **27**, pp. 3434–3446 (2020).
21. Iqbal, J., Abbasi, F.M., and Shehzad, S.A. "Heat transportation in peristalsis of Carreau-Yasuda nanofluid through a curved geometry with radial magnetic field", *Int. Commun. Heat Mass Transf.*, **177**, Article ID 104774 (2020).
22. Mahabaleshwar, U.S., Rekha, M.B., Kumar, P.N.V., et al. "Mass transfer characteristics of MHD Casson fluid flow past stretching/shrinking sheet", *J. Eng. Thermophys.*, **29**, pp. 285–302 (2020).
23. Shah, F., Khan, M.I., Chu, Y.M., et al. "Heat transfer analysis on MHD flow over a stretchable Riga wall considering entropy generation rate: A numerical study", *Numer. Methods Part. Diff. Eqs.* (2020). DOI: https://doi.org/10.1002/num.22694
24. Kiran, G.R., Shamshuddin, M.D., Krishna, C.B., et al. "Mathematical modelling of extraction of the underground fluids: application to peristaltic transportation through a vertical conduit occupied with porous material", *IOP Conf. Series: Mater. Sci. Eng.*, **981**, Article ID 022089 (2020).
25. Salawu, S.O., Kareem, R.A., Shamshuddin, M.D. et al. "Double exothermic reaction of viscous dissipative Oldroyd 8-constant fluid and thermal ignition in a channel", *Chem. Phys. Lett.*, **760**, p. 138011 (2020).
26. Shamshuddin, M.D., Salawu, S.O., Ogunseye, H.A., et al. "Dissipative power-law fluid flow using spectral quasi linearization method over an exponentially stretchable surface with Hall current and power-law slip velocity", *Int. Commun. Heat Mass Transf.*, **119**, p. 104933 (2020).
27. Akbar, Y., Abbasi, F.M., and Shehzad, S.A. "Effectiveness of Hall current and ion slip on hydromagnetic biologically inspired flow of Cu-Fe_3O_4/H_2O hybrid nanomaterial", *Phys. Scrip.*, **96**, p. 025210 (2021).
28. Tripathi, D., Prakash, J., Reddy, M.G., et al. "Numerical simulation of double diffusive convection and electroosmosis during peristaltic transport of a micropolar nanofluid on an asymmetric microchannel", *J. Therm. Anal. Calorim.*, **143**, pp. 2499–2514 (2021).
29. Tripathi, D., Prakash, J., Reddy, M.G., et al. "Numerical study of electroosmosis-induced alterations in peristaltic pumping of couple stress hybrid nanofluids through microchannel", *Ind. J. Phys.*, **95**, pp. 2411–2421 (2021).
30. Ranjit, N.K., Shit, G.C., and Tripathi, D. "Electrothermal analysis in two-layered couple stress fluid flow in an asymmetric microchannel via peristaltic pumping", *J. Therm. Anal. Calorim.*, **144**, pp. 1325–1342 (2021).
31. Selimefendigil, F. and Chamkha, A.J. "MHD mixed convection of Ag-MgO/water nanofluid in a triangular shape partitioned lid-driven square cavity involving a porous compound", *J. Therm. Anal. Calorim.*, **143**, pp. 1467–1484 (2021).
32. Abdal, S., Siddique, I., Afzal, S., et al. "On development of heat transportation through bioconvection of Maxwell nanofluid flow due to an extendable sheet with radiative heat flux and prescribed surface temperature and prescribed heat flux conditions", *Math. Methods Appl. Sci.*, (2021). DOI: https://doi.org/10.1002/mma.7722
33. Zhao, T., Khan, M.R., Chu, Y., et al. "Entropy generation approach with heat and mass transfer in magnetohydrodynamic stagnation point flow of a tangent hyperbolic nanofluid", *Appl. Math. Mech.*, **42**, pp. 1205–1218 (2021).
34. Hashmi, M.S., Khan, N., Khan, S.U., et al. "Dynamics of coupled reacted flow of Oldroyd-B material induced by isothermal/exothermal stretched disks with Joule heating, viscous dissipation and magnetic dipoles", *Alex. Eng. J.*, **60**, pp. 767–783 (2021).
35. Nazeer, M., Hussain, F., Khan, M.I., et al. "MHD two-phase flow of Jeffrey fluid suspended with Hafnium and crystal particles: Analytical treatment", *Numer. Methods Part. Diff. Eqs.* (2021). DOI: https://doi.org/10.1002/num.22766
36. Nisar, Z., Hayat, T., Alsaedi, A., et al. "Wall properties and convective conditions in MHD radiative peristalsis flow of Eyring-Powell nanofluid", *J. Therm. Anal. Calorim.*, **144**, pp. 1199–1208 (2021).
37. Rao, P.S. and Shamshuddin, M.D. "Second-order slip and Newtonian cooling impact on unsteady mixed convective radiative chemically reacting fluid with Hall current and cross-diffusion over a stretching sheet", *Heat Transf.*, **50**, pp. 7380–7405 (2021).
38. Saba, Abbasi, F.M. and Shehzad, S.A. "Heat transfer analysis for EMHD peristalsis of ionic-nanofluids via curved channel with Joule dissipation and Hall effects", *J. Biolog. Phys.*, **47**, pp. 455–476 (2021).
39. Akram, J., Akbar, N.S., and Tripathi, D. "Thermal analysis on MHD flow of ethylene glycol-based BNNTs nanofluids via peristaltically induced electroosmotic pumping in a curved microchannel", *Arab. J. Sci. Eng.*, **47**, pp. 7487–7503 (2022).
40. Akram, J., Akbar, N.S., and Tripathi, D. "Entropy generation in electroosmotically aided peristaltic pumping of MoS_2 Rabinowitsch nanofluid", *Fluid Dyn. Res.*, **54**, Article ID 015507 (2022).
41. Akram, J., Akbar, N.S., and Tripathi, D. "Electroosmosis augmented MHD peristaltic transport of SWCNTs suspension in aqueous media", *J. Therm. Anal. Calorim.*, **147**, pp. 2509–2526 (2022).
42. Luciano, M., Xue, S.L., De Vos, W.H., et al. "Large-scale curvature sensing by epithelial monolayers depends on active cell mechanics and nuclear mechanoadaptation", *Nature Phys.*, **17**, pp. 1382–1390 (2021).

43. Callens, S.J., Uyttendaele, R.J., Fratila-Apachitei, L.E., et al. "Substrate curvature as a cue to guide spatiotemporal cell and tissue organization", *Biomater.*, **232**, p. 119739 (2020).
44. Augustin, C.M., Fastl, T.E., Neic, A., et al. "The impact of wall thickness and curvature on wall stress in patient-specific electromechanical models of the left atrium", *Biomech. Model. Mechanobiology*, **19**, pp. 1015–1034 (2020).
45. Saba, Abbasi, F.M. and Shehzad, S.A. "Impact of curvature-dependent channel walls on peristaltic flow of Newtonian fluid through a curved channel with heat transfer", *Arab. J. Sci. Eng.*, **45**, pp. 9037–9044 (2020).

Biographies

Saba is working as PhD scholar at Department of Mathematics, COMSATS University Islamabad, Islamabad Campus, Pakistan. She has published 4 research articles in International journals. Her research area is peristaltic flow of Newtonian and Non-Newtonian fluids through different flow geometries.

Sabir Ali Shehzad is working as an Associate Professor at Department of Mathematics, COMSATS University Islamabad, Sahiwal, Pakistan. He has completed his PhD in Fluid Mechanics from Quaid-I-Azam University, Islamabad, Pakistan in 2014. His main research interests are Newtonian and non-Newtonian fluids, nanofluids and heat and mass transfer analysis. He has published more than 300 research articles in various high reputed international journals. He is reviewer of more than 100 international journals.

Fahad Munir Abbasi is working as an Associate Professor at Department of Mathematics, COMSATS University Islamabad, Islamabad Campus, Pakistan. He has completed his PhD in Fluid Mechanics from Quaid-I-Azam University, Islamabad, Pakistan. His main research interests are peristaltic flow, numerical modeling, Newtonian and non-Newtonian fluids. He has published $>$ 100 research articles in various high reputed international journals. He is also reviewer of more than 50 International journals.